Coherent Excitation of Heterosymmetric Spin Waves with Ultrashort Wavelengths

G. Dieterle,[1,*] J. Förster,[1] H. Stoll,[1,2] A. S. Semisalova,[3,¶] S. Finizio,[4] A. Gangwar,[5] M. Weigand,[1,†] M. Noske,[1] M. Fähnle,[1] I. Bykova,[1] J. Gräfe,[1] D. A. Bozhko,[6,‡] H. Yu. Musiienko-Shmarova,[6] V. Tiberkevich,[7] A. N. Slavin,[7] C. H. Back,[5,§] J. Raabe,[4] G. Schütz,[1] and S. Wintz[3,4,‖]

[1]*Max-Planck-Institut für Intelligente Systeme, 70569 Stuttgart, Germany*
[2]*Johannes Gutenberg-Universität Mainz, 55128 Mainz, Germany*
[3]*Helmholtz-Zentrum Dresden-Rossendorf, 01328 Dresden, Germany*
[4]*Paul Scherrer Institut, 5232 Villigen PSI, Switzerland*
[5]*Universität Regensburg, 93053 Regensburg, Germany*
[6]*Technische Universität Kaiserslautern, 67663 Kaiserslautern, Germany*
[7]*Oakland University, Rochester, Michigan 48309, USA*

(Received 28 November 2018; published 21 March 2019)

In the emerging field of magnonics, spin waves are foreseen as signal carriers for future spintronic information processing and communication devices, owing to both the very low power losses and a high device miniaturization potential predicted for short-wavelength spin waves. Yet, the efficient excitation and controlled propagation of nanoscale spin waves remains a severe challenge. Here, we report the observation of high-amplitude, ultrashort dipole-exchange spin waves (down to 80 nm wavelength at 10 GHz frequency) in a ferromagnetic single layer system, coherently excited by the driven dynamics of a spin vortex core. We used time-resolved x-ray microscopy to directly image such propagating spin waves and their excitation over a wide range of frequencies. By further analysis, we found that these waves exhibit a heterosymmetric mode profile, involving regions with anti-Larmor precession sense and purely linear magnetic oscillation. In particular, this mode profile consists of dynamic vortices with laterally alternating helicity, leading to a partial magnetic flux closure over the film thickness, which is explained by a strong and unexpected mode hybridization. This spin-wave phenomenon observed is a general effect inherent to the dynamics of sufficiently thick ferromagnetic single layer films, independent of the specific excitation method employed.

DOI: 10.1103/PhysRevLett.122.117202

Spin waves are the collective excitations of magnetically ordered spin systems, with the "magnon" being their fundamental quantum of excitation [1–3]. In a simplified view, a spin wave can be regarded as a collective precession of the magnetization ($\boldsymbol{M}$) with a periodic spatial phase shift [Fig. 1(a)], imposing the wavelength λ and, inversely, the wave vector $\boldsymbol{k} = (2\pi/\lambda)\boldsymbol{e_k}$, with $\boldsymbol{e_k}$ corresponding to the propagation direction of phase fronts. Taking into account the precession frequency f, the phase velocity of a spin wave is determined by $v = \lambda f$. Depending on the underlying magnetic system, spin waves cover a wide spectral band, up to the THz range with wavelengths extending from macroscopic length scales to the subnanometer domain [4,5]. While spin waves also occur in three-dimensional bulk systems, the main focus of magnonics research is set on quasi-two-dimensional and technologically more relevant thin films.

The two main advantages of using spin waves over present charge-based technologies are a substantially lower power dissipation (preventing Ohmic losses) and a high device miniaturization potential owing to the orders of magnitude shorter wavelengths of spin waves compared to that of electromagnetic waves [4–14].

Typical methods to excite spin waves coherently in magnetic thin films utilize nonlinear parametric pumping by uniformly alternating magnetic fields [9,14], patterned conductive antennas as microwave to spin-wave transducers [7,8,14], or current induced spin-transfer torques in nanocontact geometries [9,10,12]. While parametric pumping, however, suffers from a cumbersome tunability of the excited wavelengths, the two other methods mentioned fail to efficiently generate spin waves with wavelengths below the patterning sizes involved [14]. Recently, the latter limitation was partially overcome in specific magnetic systems by—when categorized in general terms—making use of Fano resonances [6,11,15–18], the Schlömann mechanism [19–23], or a postexcitation variation of the magnonic index [24–26]. Yet, for the technologically most relevant plain thin film geometry, the demand for high amplitude ultrashort spin-wave excitation sources remains unanswered at present.

Generally, the dispersion relation $f(k)$ of spin waves is mainly determined by the magnetodipole and the exchange interaction, where the first one is dominant in the long wavelength limit and the second governs the regime of ultrashort waves [14,27–29]. In magnetic thin films, the dispersion relation strongly depends on the relative orientation of the propagation direction and the static equilibrium magnetization. For in-plane magnetized films, there is a distinction between the backward volume ($\boldsymbol{k}\|\boldsymbol{M}$) and the Damon-Eshbach ($\boldsymbol{k}\perp\boldsymbol{M}$) geometry, the latter typically

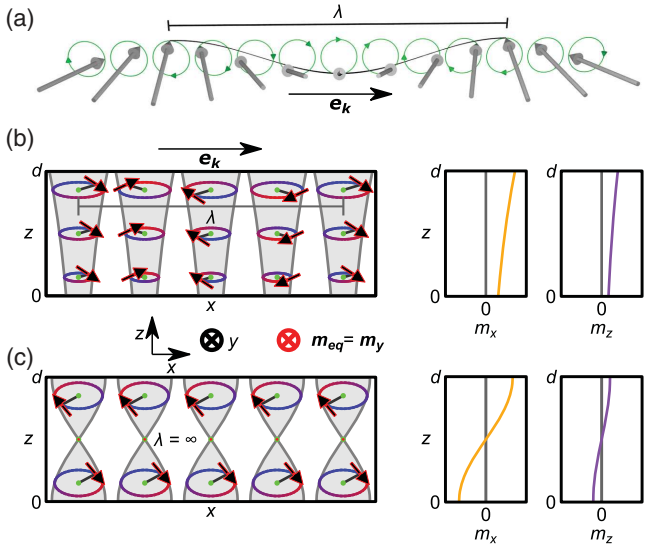

FIG. 1. Schematics of spin waves. (a) Spin wave propagating along $\boldsymbol{e_k}$. Magnetic moments (gray arrows) precessing with a spatial phase difference determining the wavelength $\boldsymbol{\lambda}$. (b) Cross-sectional precession profile of a quasi-uniform Damon-Eshbach spin wave in a thin film of thickness $\boldsymbol{d}$, with finite lateral wavelength, propagating along $\boldsymbol{e_k}$. (c) Cross-sectional precession profile of the first perpendicular standing spin-wave mode for free surface boundary conditions and with laterally uniform magnetization precession (infinite lateral wavelength). Right panels: Separated profiles of the corresponding dynamic $\boldsymbol{m_x}$ (yellow line) and $\boldsymbol{m_z}$ (purple line) components.

exhibiting higher phase velocities and positive group velocities [14,30], making it preferable for signal transmission applications.

While principally being of surface wave nature with an exponentially decaying thickness profile in bulk samples [30], Damon-Eshbach waves exhibit an almost uniform distribution of the wave amplitude over the film thickness in thin films with thicknesses d much smaller than λ [cf. Fig. 1(b)]. Such waves have been investigated by optical means, namely, magneto-optical Kerr microscopy [31] and Brillouin light scattering [32], down to wavelengths at the optically accessible limit of $\lambda \sim 250$ nm. Additionaly, exchange dominated higher-order spin waves with nonuniform mode profiles over the film thickness occur at higher frequencies due to vertical confinement effects. Such modes are typically observed in ferromagnetic resonance experiments as perpendicular standing waves for the nonpropagating case of laterally uniform precession ($\lambda_{xy} \to \infty$) [33,34], and are characterized by their number of precession nodes along the film thickness [cf. Fig. 1(c)] [27,28]. Nevertheless, also first experimental evidences have been found for laterally propagating higher-order waves of finite λ [27–29,35,36], by means of spectroscopically detecting thermally excited incoherent magnons [37–39] or even coherent waves yet only in the long wavelength limit [40–42].

In this Letter, we show that high-amplitude, ultrashort ($\lambda \sim 100$ nm) propagating spin waves can be excited in a single layer magnetic thin film with a thickness of the order of 100 nm by a nanoscopic magnetic vortex core. For this excitation process, pioneered recently in a multilayered heterosystem [6], the vortex core is driven to gyration by applying alternating external magnetic fields with frequencies of the order of $f \sim 10$ GHz, and the resulting spin-wave wavelength was found to be directly tunable by the driving frequency. We used time-resolved magnetic x-ray microscopy to image the effects of spin-wave emission and propagation. By further analysis, we show that the observed spin waves correspond to the first higher-order mode (having one thickness node) in the Damon-Eshbach geometry. Interestingly, the thickness profile of the observed mode is found to be influenced by a significant mode hybridization and therefore is of heterosymmetric character with respect to the perpendicular (symmetric) and lateral (antisymmetric) dynamic magnetization components. Thus, the excited spin-wave mode exhibits points of purely linear magnetic oscillations and regions with anti-Larmor precession sense.

Our experimental sample is a Permalloy ($Ni_{81}Fe_{19}$) circular thin film disc with a lateral diameter of 3 μm and a thickness of $d = 80$ nm [cf. Supplemental Material [43], (1)]. The expected magnetic ground state for this sample is a topological spin vortex with flux-closing in-plane magnetization circulation and a perpendicularly oriented nanoscopic vortex core in the center [54]. We verified the sample to exibit a vortex state by imaging its local magnetic orientation $\boldsymbol{m} = \boldsymbol{M}/M$ using scanning transmission x-ray microscopy (cf. Supplemental Material [43]). Figure 2(a) shows a microscopy image with lateral m_x sensitivity (white: $+m_x$, black: $-m_x$) revealing the in-plane magnetic orientation in the disc.

The sample was excited by in-plane magnetic fields $B_{\mathrm{ext},y}(t) = B_{\mathrm{ext},y0}\sin(2\pi f t)$ alternating in time t. We directly imaged the dynamic response $\boldsymbol{m}(t)$ in the disc by stroboscopic, time-resolved scanning transmission x-ray microscopy in the frequency range from 5.6 to 10.1 GHz. Figure 2(b) displays a snapshot of such a dynamic response with perpendicular m_z magnetic sensitivity to an excitation with a frequency of $f = 7.4$ GHz and an amplitude of $B_{\mathrm{ext}} \sim 1$ mT. The vortex core is clearly visible as a black dot in the center. Moreover, a radial spin-wave pattern is observed, with highest amplitudes in the vicinity of the core (cf. magnified inset), decaying towards the edge of the disc. This spin-wave pattern is further highlighted in a normalized view [cf. Fig. 2(c)], showing the temporal perpendicular magnetic deviations. The full dynamic microscopy image sets, provided as movies (M1-M6) in the Supplemental Material [43], reveal that the observed spin waves are emitted from the vortex core. Driven by the alternating magnetic field, the gyrating vortex core dynamically induces dips of same and opposite magnetic orientation [55–59] locally, thereby coherently exciting propagating waves [6] [cf. Supplemental Material [43] (3d)], as further confirmed by micromagnetic simulations (cf. Supplemental Material [43] M7). Abstractly,

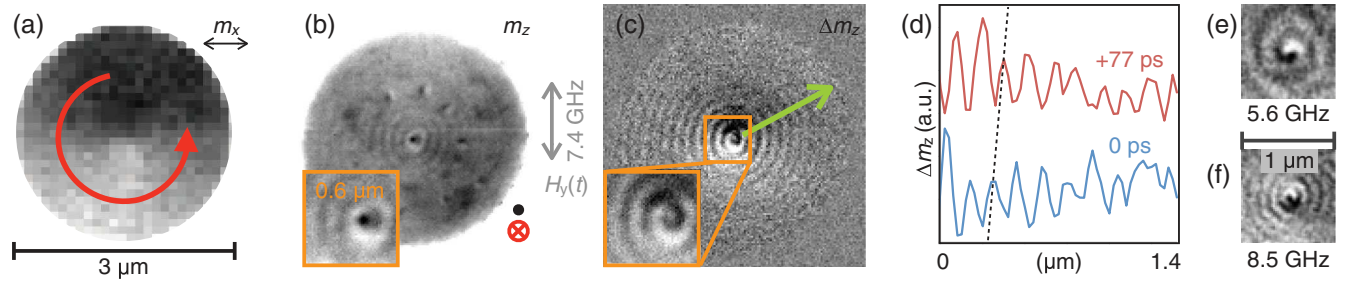

FIG. 2. Emission of ultrashort spin waves from a magnetic vortex core. (a) X-ray microscopy image showing the static in-plane magnetic vortex configuration of the disc with the red arrow indicating the magnetic orientation. (b,c) Time-resolved x-ray microscopy images (snapshots) with out-of-plane sensitivity showing the response of the sample to an in-plane alternating magnetic field excitation of $f = 7.4$ GHz. (b) Absolute absorption images (full sample and magnified center region) revealing the vortex core in the center (black dot) and a radial spin-wave pattern with $\lambda = 140$ nm. (c) Normalized images showing only the temporal magnetic changes with respect to the average state, clearly highlighting the spin-wave spiral emitted. (d) Line profiles along the green arrow in (c) at a relative time delay of 77 ps (from blue to red curve) illustrating wave propagation. (e) and (f) Normalized x-ray images showing $\Delta m_z(t)$ for excitation frequencies of $f = 5.6$ and $f = 8.5$ GHz, respectively.

this effect can be considered a local Fano resonance [15] of the discrete core gyration mode with the continuum of propagating spin waves, mediated via a coherent, linear coupling. Note that such linear coherent spin-wave generation does not result from a frequency-doubling mechanism [60] and fundamentally differs from the incoherent spin-wave excitation by dynamic vortex core reversal [61,62]. Once excited, the spin waves in our experiment propagate radially towards the edge of the disc, i.e., perpendicular to the azimuthal vortex equilibrium magnetization, which formally corresponds to the Damon-Eshbach geometry ($\boldsymbol{k} \perp \boldsymbol{M}$). Along with the continuous phase difference of the spin waves emitted during gyration, this leads to the formation of a spiral pattern (cf. Ref. [43]). The propagation is visualized by line profiles [along the green arrow in Fig. 2(c)] for a relative time delay of 77 ps [blue and red lines in Fig. 2(d)]. From this graph we conclude that the spin-wave amplitude exhibits very high values in the vicinity of the core [$m_z \approx 0.25$, cf. Fig. 2(d), Supplemental Material [43] M1] and that the wavelength is about 140 nm.

Moreover, we found that the wavelengths of such excited spin waves are continuously tunable by changing the driving frequency in the range from 5.6 to 10.1 GHz without the need of any external magnetic bias field, as shown in Figs. 2(e) and 2(f) exemplarily for ($f = 5.6$ GHz, $\lambda = 250$ nm) and ($f = 8.5$ GHz, $\lambda = 110$ nm). This wide-band process of vortex core driven spin-wave generation, observed in a single magnetic layer, underlines the universality of the effect of spin-wave emission from confined noncollinear spin textures such as domain walls [60,63–66] and vortex cores, where the latter had only been reported for a highly specific multilayered heterosystem so far [6]. Moreover, the spin-wave frequencies found here (exceeding 10 GHz), are substantially higher than those observed previously [6], the corresponding wavelengths clearly attaining the ultrashort (sub-100 nm) regime. Note that the observed spin waves are not eigenmodes of the disc [57], but independent from the lateral dimensions [cf. Supplemental Material [43] (3c)].

The spin-wave dispersion relation $f(k)$ of the experimentally observed spin waves (cf. Fig. 3, red dots) exhibits an almost linear behavior at a constant group velocity of $v_g = d\omega/dk = 550$ m/s in the k range given $(25 < k < 80)$ rad/μm, where $\omega = 2\pi f$ is the angular frequency. Remarkably, this dispersion qualitatively differs from the analytically calculated zeroth order, quasi-uniform (for $k < 25$ rad/μm) Damon-Eshbach dispersion [27,28] [cf. Supplemental Material [43] (4)], (see blue line in Fig. 3) typically investigated.

Furthermore, higher-order perpendicular standing spin-wave modes observed for the case of laterally uniform precession ($\lambda_{xy} \to \infty$) [33,34] are predicted to extend to the regime of laterally propagating dipole-exchange waves of finite λ_{xy}. We therefore analytically calculated [27] (cf. methods) the dispersion relations of both the first ($p = 1$) and the second ($p = 2$) of these higher-order modes (red and green lines in Fig. 3), respectively, with p being the ordinal index of nodes in the mode thickness profile at zero lateral wave number $k_{xy} = 0$ [27]. The analytical dispersion relation $f_1(k)$ clearly matching the experimental one, we identify the experimentally observed spin-wave mode as the first higher-order propagating mode. The excellent agreement of both experimental and analytical results with micromagnetic simulations [blue triangles: quasi-uniform mode, red crosses: first higher-order mode in Fig. 3, Supplemental Material [43] (5)] further supports this experimental observation of coherent, higher-order propagating spin waves. Moreover, the simulations show that, in the given (f, k) range, the dispersion relations for plane spin waves in a continuous thin film and for radial waves in a magnetic vortex state are practically identical [cf. Supplemental Material [43] (5)], underlining the general validity of our findings. Additionally, also quasi-uniform waves with longer wavelengths ($\lambda > 200$ nm) are principally exciteable in the disc structures used [cf. Supplemental Material [43] (5)]. However,

these waves are not excited by vortex core gyration but stem from the magnetic discontinuity at the rim.

Generally, hybridization (or mixing) between modes having different ordinal indices p negligibly influences their dispersion relations up to moderate k values. However, hybridization might become relevant for higher k values and is crucial in the vicinity of mode crossing points, eventually leading to avoided crossings when hybridization is included analytically (cf. inset Fig. 3) [27]. Yet neglecting hybridization, the dispersion relations $f_p(k)$ of the dipole-exchange modes of higher-order ($p \geq 1$) can be analytically calculated, yielding for the case of free surface boundary conditions [Ref. [27], Supplemental Material [43] (4a)]

$$f_p(k) = \frac{\gamma\mu_0}{2\pi}\sqrt{\left\{\frac{2A}{\mu_0 M_S}\left[k^2 + \left(\frac{p\pi}{d}\right)^2\right]\right\}\left\{\frac{2A}{\mu_0 M_S}\left[k^2 + \left(\frac{p\pi}{d}\right)^2\right] + M_S\right\}}, \quad (1)$$

with μ_0 being the vacuum permeability, $\gamma = 176.8$ GHz/T the gyromagnetic ratio, and $A = 0.75 \times 10^{-11}$ J/m the exchange constant [cf. Supplemental Material [43] (4)]. Note that the dispersion relations $f_p(k)$ strongly depend on both A and d; i.e., these relations can be efficiently tuned by varying these parameters [cf. Supplemental Material [43] (4)].

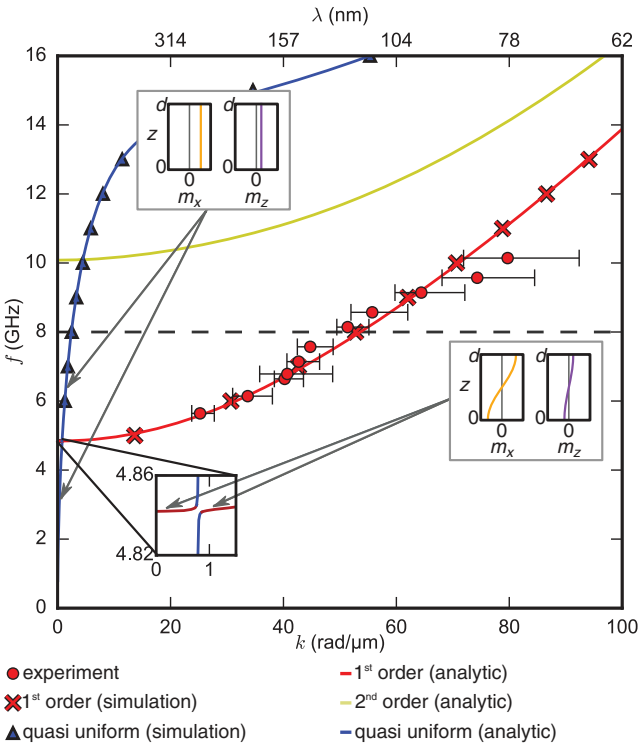

FIG. 3. Spin-wave dispersion relations $f(k)$. Solid red dots correspond to the experimental data points measured in a single layer vortex structure, solid lines to the analytically calculated dispersion curves of the quasi-uniform branch (blue) and the *first* (red) and *second* (green) higher-order branches, considering mode hybridization. Results from micromagnetic simulations are marked as blue triangles (quasi-uniform mode) and red crosses (first higher-order mode). The inset shows the calculated avoided mode crossing of the dispersion curves. Schematic mode profiles for certain dispersion points are shown as yellow (dynamic m_x component) and purple (dynamic m_z component) lines. The dashed horizontal line indicates a frequency of 8 GHz.

Remarkably for sufficiently thick layers, as in this case, the first higher-order spin-wave dispersion above a certain frequency (here ~5 GHz) exhibits significantly larger k values than the quasi-uniform Damon-Eshbach dispersion (cf. Fig. 3). For k values above ~1 rad/μm, equivalently, the frequency (and thus magnon energy) of the first higher-order spin-wave mode is lower than that of the quasi-uniform one. This contrasts with ferromagnetic resonance experiments ($\lambda_{xy} \to \infty$) and traveling waves in ultrathin films, where higher-order perpendicular standing waves solely occur at frequencies above that of the uniform precession or quasi-uniform propagation [33,34].

In order to qualitatively understand the characteristics of the observed dispersion law, we evaluated the simulated thickness profiles for both the quasi-uniform [cf. Figs. 4(a)–4(c)] and the first higher-order spin-wave mode [cf. Figs. 4(d)–4(f)] at a frequency of 8 GHz (dotted horizontal line in Fig. 3). With the static equilibrium magnetization $\boldsymbol{m}_{\mathbf{eq}} = +\boldsymbol{m}_y$ (into the paper plane), the top (middle) panels of Fig. 4 show the thickness distribution of the dynamic magnetization components m_z (m_x) at a fixed time, while the bottom panels display the corresponding precession orbits and phases. Analyzing the quasi-uniform spin-wave profile with a lateral wavelength of ~2 μm, confirms that both dynamic magnetization components m_z [Fig. 4(a)] and m_x [Fig. 4(b)] are distributed almost uniformly over the film thickness, slightly decaying from the top to the bottom surface only. Thus, the precession phase [Fig. 4(c)] is constant over the film thickness, and the precession always obeys to the Larmor sense, i.e., a right-handed precession with respect to $\boldsymbol{m}_{\mathbf{eq}}$.

This situation fundamentally changes for the first higher-order mode, exhibiting a more than 20 times shorter wavelength of only ~100 nm at the same frequency. Here, the maximum amplitude of the dynamic magnetic m_z component is located slightly below the center of the film, the amplitude decaying towards both surfaces [cf. Fig. 4(d)]. The dynamic m_x-component profile [cf. Fig. 4(e)] of the higher-order mode, however, exhibits a nodal line of zero m_x

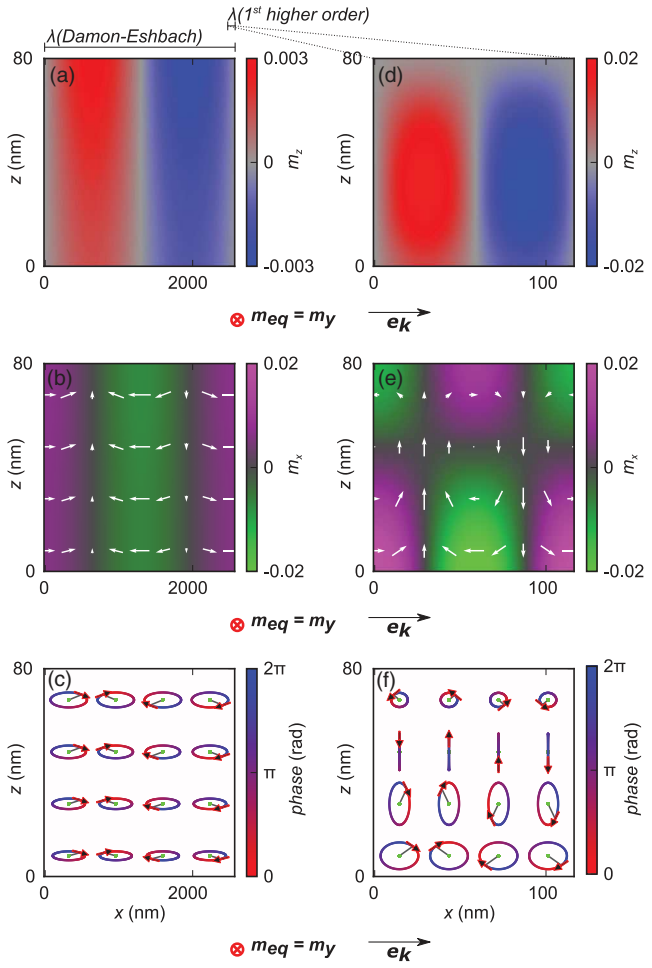

FIG. 4. Spin-wave thickness profiles from micromagnetic simulations at $f = 8$ GHz. The left column (a)–(c) shows the quasi-uniform branch, while the right column (d)–(f) shows the first higher-order branch. (a),(d) display snapshots of the dynamic m_z components as red and blue contrast (spatially smoothed). (b), (e) show the corresponding dynamic m_x components collinear to $\boldsymbol{e_k}$ as red and green contrast (spatially smoothed), with additional indication of both dynamic magnetic components as white arrows. (c),(f) show the position dependent (green points) precession orbit and the precession sense and phase.

amplitude slightly above the film center. Above and below this line, the corresponding m_x components exhibit an antiphase relation, their amplitudes increasing towards both surfaces. In the same panel, arrows indicate the local $m_{x,z}$ components, revealing the dynamic magnetization to follow a flux closing, thus stray-field reducing, vortex over the film thickness. Laterally these vortices alternate in their circulation sense (one pair per wavelength) with their propagating cores showing zero dynamic components ($\boldsymbol{m} = \boldsymbol{m}_y$). This heterosymmetric mode profile (0 m_z nodes, 1 m_x node) has crucial implications for the local magnetization precession [cf. Fig. 4(f)]. While below the m_x-nodal line a mildly elliptic precession with Larmor sense is observed, the magnetization on the nodal line itself purely linearly oscillates along the z axis. Most strikingly, however, the precession exhibits a reversed Larmor sense above the nodal line. Although such local anti-Larmor precession was theoretically predicted already in the 1970s [36] and thereafter discussed related to incoherent thermal magnon measurements [35], it had not been experimentally verified for short-wavelength coherent spin waves so far. Note that such behavior also qualitatively differs from the higher-order modes both observed in ferromagnetic resonance experiments and analytically calculated neglecting mode hybridization, for which the precession always has Larmor sense. However, when analytically considered [Ref. [27], Supplemental Material [43] 4(a)], the hybridization of modes of different order p can be cleardly identified as origin for the peculiar mode profiles discussed, revealing the crucial role of mode hybridization at higher k values even far away from their avoided crossings.

In summary, we observed the coherent excitation of high-amplitude spin waves with sub-100 nm wavelengths by the driven nonresonant gyration of topologically stabilized magnetic vortex cores in single layer magnetic thin film structures. This excitation mechanism does not require any magnetic bias field and persists over a wide frequency range exceeding 10 GHz. Directly imaging the corresponding spin-wave propagation by time-resolved scanning transmission x-ray microscopy, revealed an almost linear dispersion above $k \gtrsim 25$ rad/μm with group velocities of approximately 500 m/s. The experimental results were fully reproduced by micromagnetic simulations, and the observed wave mode was identified as first higher-order propagating dipole-exchange spin-wave mode of the Damon-Eshbach geometry, predicted earlier by analytic theory. Remarkably, for sufficiently thick films, this first higher-order mode exhibits substantially lower frequencies than the quasi-uniform Damon-Eshbach mode below a certain wavelength [cf. Supplemental Material [43] (4c) [43]]. Furthermore, we found that because of significant mode hybridization, the thickness profile of the observed mode is heterosymmetric, leading to the formation of flux closing, thus strayfield reducing, dynamic magnetic vortices over the film profile as well as to regions with anti-Larmor precession sense. Apart from their fundamental importance and perspectives (such as to study k-dependent dissipation mechanisms for ultrashort spin waves), our findings may open a new chapter for magnon spintronics, by meeting the demand for confined, efficient, and tunable sources of coherent ultrashort spin waves in the GHz range.

We would like to thank R. Verba and J. Lindner for fruitful discussions, M. Bechtel for experimental support at the MAXYMUS STXM beam line, K. Hahn and U. Eigenthaler for the TEM measurements, and R. Mattheis for his help with the sample fabrication. Support by the Nanofabrication Facilities Rossendorf at IBC and by the Laboratory for Micro- and Nanotechnology at PSI is gratefully acknowledged. The experiments were performed at the MAXYMUS endstation at BESSY II in Berlin, Germany. We thank the

HZB for the allocation of synchrotron radiation beam time. S. F. acknowledges funding from the EU Horizon 2020 project MAGicSky (Grant No. 665095). V. T. and A. N. S. acknowledge funding by the Grant No. EFMA-1641989 from the National Science Foundation of the USA, by the grant from DARPA, and by the grant from the Center for NanoFerroic Devices (CNFD) and Nanoelectronics Research Initiative (NRI). D. A. B. and H. Yu. M.-S. acknowledge support by the DFG within Spin +X SFB/TRR 173. S. W. acknowledges funding from the European Community's Seventh Framework Programme (FP7/2007-2013) under Grant Agreement No. 290605 (PSI-FELLOW/COFUND).

*dieterle@is.mpg.de
†Present address: Helmholtz-Zentrum Berlin für Materialien und Energie, 12489 Berlin, Germany.
‡Present address: Glasgow University, Glasgow G12 8LT, United Kingdom.
§Present address: Technische Universität München, 85748 München, Germany.
‖sebastian.wintz@psi.ch
¶Present address: Universität Duisburg-Essen, 47057 Duisburg, Germany.

[1] F. Bloch, Zur Theorie des Ferromagnetismus, Z. Phys. **61**, 206 (1930).
[2] T. Holstein and H. Primakoff, Field dependence of the intrinsic domain magnetization of a ferromagnet, Phys. Rev. **58**, 1098 (1940).
[3] F. J. Dyson, General theory of general spin wave interactions, Phys. Rev. **102**, 1217 (1956).
[4] A. V. Chumak, V. I. Vasyuchka, A. A. Serga, and B. Hillebrands, Magnon spintronics, Nat. Phys. **11**, 453 (2015).
[5] V. V. Kruglyak, S. O. Demokritov, and D. Grundler, Magnonics, J. Phys. D **43**, 264001 (2010).
[6] S. Wintz, V. Tyberkevych, M. Weigand, J. Raabe, J. Lindner, A. Erbe, A. N. Slavin, and J. Fassbender, Magnetic vortex cores as tunable spin wave emitters, Nat. Nanotechnol. **11**, 948 (2016).
[7] A. Haldar, D. Kumar, and A. O. Adeyeye, A reconfigurable waveguide for energy-efficient transmission and local manipulation of information in a nanomagnetic device, Nat. Nanotechnol. **11**, 437 (2016).
[8] K. Wagner, A. Kákay, K. Schultheiss, A. Henschke, T. Sebastian, and H. Schultheiss, Magnetic domain walls as reconfigurable spin-wave nanochannels, Nat. Nanotechnol. **11**, 432 (2016).
[9] V. E. Demidov, S. Urazhdin, and S. O. Demokritov, Direct observation and mapping of spin-waves emitted by spin-torque nano-oscillators, Nat. Mater. **9**, 984 (2010).
[10] M. Madami, S. Bonetti, G. Consolo, S. Tacchi, G. Carlotti, G. Gubbiotti, F. B. Mancoff, M. A. Yar, and J. Åkerman, Direct observation of a propagating spin wave induced by spin-transfer torque, Nat. Nanotechnol. **6**, 635 (2011).
[11] H. Yu, O. d' Allivy Kelly, V. Cros, R. Bernard, P. Bortolotti, A. Anane, F. Brandl, F. Heimbach, and D. Grundler, Approaching soft X-ray wavelengths in nanomagnet-based microwave technology, Nat. Commun. **7**, 11255 (2016).
[12] S. Urazhdin, V. E. Demidov, H. Ulrichs, T. Kendziorczyck, T. Kuhn, J. Lethold, G. Wilde, and S. O. Demokritov, Nanomagnetic devices based on the spin-transfer torque, Nat. Nanotechnol. **9**, 509 (2014).
[13] K. Vogt, F. Y. Fradin, J. E. Pearson, T. Sebastian, S. D. Bader, B. Hillebrands, A. Hoffmann, and H. Schultheiss, Realization of a spin-wave multiplexer, Nat. Commun. **5**, 3727 (2014).
[14] A. G. Gurevich and G. A. Melkov, *Magnetization Oscillations and Waves* (CRC, New York, 1996).
[15] U. Fano, Effects of configuration interaction on intensities and phase shifts, Phys. Rev. **124**, 1866 (1961).
[16] Y. Au, E. Ahmad, O. Dmytriiev, M. Dvornik, T. Davison, and V. V. Kruglyak, Resonant microwave-to-spin-wave transducer, Appl. Phys. Lett. **100**, 182404 (2012).
[17] H. Yu, G. Duerr, R. Huber, M. Bahr, T. Schwarze, F. Brandl, and D. Grundler, Omnidirectional spin-wave nanograting coupler, Nat. Commun. **4**, 2702 (2013).
[18] S. J. Hämäläinen, F. Brandl, K. J. A. Franke, D. Grundler, and S. van Dijken, Tunable short-wavelength spin-wave emission and confinement in anisotropy-modulated multiferroic heterostructures, Phys. Rev. Applied **8**, 014020 (2017).
[19] E. Schlömann, Generation of spin-waves in nonuniform magnetic fields, I. Conversion of electromagnetic power into spin-wave power and vice versa, J. Appl. Phys. **35**, 159 (1964).
[20] F. B. Mushenok, R. Dost, C. S. Davies, D. A. Allwood, B. J. Inkson, G. Hrkac, and V. V. Kruglyak, Broadband conversion of microwaves into propagating spin-waves in patterned magnetic structures, Appl. Phys. Lett. **111**, 042404 (2017).
[21] C. S. Davies, A. V. Sadovnikov, S. V. Grishin, Yu. P. Sharaevskii, S. A. Nikitov, and V. V. Kruglyak, Generation of propagating spin-waves from regions of increased dynamic demagnetising field near magnetic antidots, Appl. Phys. Lett. **107**, 162401 (2015).
[22] C. S. Davies and V. V. Kruglyak, Generation of propagating spin-waves from edges of magnetic nanostructures pumped by uniform microwave magnetic field, IEEE Trans. Magn. **52**, 2300504 (2016).
[23] C. S. Davies, V. D. Poimanov, and V. V. Kruglyak, Mapping the magnonic landscape in patterned magnetic structures, Phys. Rev. **96**, 094439 (2017).
[24] C. S. Davies, A. Francis, A. V. Sadovnikov, S. V. Chertopalov, M. T. Bryan, S. V. Grishin, D. A. Allwood, Y. P. Sharaevskii, S. A. Nikitov, and V. V. Kruglyak, Towards graded-index magnonics: Steering spin-waves in magnonic networks, Phys. Rev. B **92**, 020408(R) (2015).
[25] V. E. Demidov, M. P. Kostylev, K. Rott, J. Münchenberger, G. Reiss, and S. O. Demokritov, Excitation of short-wavelength spin-waves in magnonic waveguides, Appl. Phys. Lett. **99**, 082507 (2011).
[26] J. Stigloher, M. Decker, H. S. Körner, K. Tanabe, T. Moriyama, T. Taniguchi, H. Hata, M. Madami, G. Gubbiotti, K. Kobayashi, T. Ono, and C. H. Back, Snell's Law for Spin-Waves, Phys. Rev. Lett. **117**, 037204 (2016).
[27] B. A. Kalinikos and A. N. Slavin, Theory of dipole-exchange spin wave spectrum for ferromagnetic films with

mixed exchange boundary conditions, J. Phys. C **19**, 7013 (1986).
[28] R. E. Arias, Spin-wave modes of ferromagnetic films, Phys. Rev. B **94**, 134408 (2016).
[29] M. Kostylev, Non-reciprocity of dipole-exchange spin-waves in thin ferromagnetic films, J. Appl. Phys. **113**, 053907 (2013).
[30] R. W. Damon and J. R. Eshbach, Magnetostatic modes of a ferromagnetic slab, J. Phys. Chem. Solids **19**, 308 (1961).
[31] J. P. Park, P. Eames, D. M. Engebretson, J. Berezovsky, and P. A. Crowell, Spatially Resolved Dynamics of Localized Spin-Wave Modes in Ferromagnetic Wires, Phys. Rev. Lett. **89**, 277201 (2002).
[32] J. R. Sandercok and W. Wettling, Light scattering from thermal acoustic magnons in yttrium iron garnet, Solid State Commun. **13**, 1729 (1973).
[33] C. Kittel, Excitation of spin-waves in a ferromagnet by a uniform rf field, Phys. Rev. **110**, 1295 (1958).
[34] M. H. Seavey, Jr. and P. E. Tannenwald, Direct Observation of Spin Wave Resonance, Phys. Rev. Lett. **1**, 168 (1958).
[35] P. Grünberg, M. G. Cottam, W. Vach, C. Mayr, and R. E. Camley, Brillouin scattering of light by spin-waves in thin ferromagnetic films (invited), J. Appl. Phys. **53**, 2078 (1982).
[36] N. M. Salansky and M. Sh. Erukhimov, *Fizicheskiye Svoystva i Primeneniya Magnitnykh Plenok [Physical Properties and Application of Magnetic Films]* (Nauka, Novosibirsk, 1975).
[37] P. Kabos, W. D. Wilber, C. E. Patton, and P. Grünberg, Brillouin light scattering study of magnon branch cross over in thin iron films, Phys. Rev. B **29**, 6396 (1984).
[38] J. Jorzick, S. O. Demokritov, C. Mathieu, B. Hillebrands, B. Bartenlian, C. Chappert, F. Rousseaux, and A. N. Slavin, Brillouin light scattering from quantized spin-waves in micron-size magnetic wires, Phys. Rev. B **60**, 15194 (1999).
[39] O. Gaier, J. Hamrle, S. Trudel, A. Conca Parra, B. Hillebrands, E. Arbelo, C. Herbort, and M. Jourdan, Brillouin light scattering study of $Co_2Cr_{0.6}Fe_{0.4}Al$ and Co_2FeAl Heusler compounds, J. Phys. D **42**, 084004 (2009).
[40] A. A. Serga, A. V. Chumak, A. André, G. A. Melkov, A. N. Slavin, S. O. Demokritov, and B. Hillebrands, Parametrically Stimulated Recovery of a Microwave Signal Stored in Standing Spin-Wave Modes of a Magnetic Film, Phys. Rev. Lett. **99**, 227202 (2007).
[41] S. Schäfer, A. V. Chumak, A. A. Serga, G. A. Melkov, and B. Hillebrands, Microwave spectral analysis by means of nonresonant parametric recovery of spin-wave signals in a thin magnetic film, Appl. Phys. Lett. **92**, 162514 (2008).
[42] S. Schäfer, V. Kegel, A. A. Serga, B. Hillebrands, and P. Kostylev, Variable damping and coherence in a high-density magnon gas, Phys. Rev. B **83**, 184407 (2011).
[43] See Supplemental Material at http://link.aps.org/supplemental/10.1103/PhysRevLett.122.117202 for methods, results of further micromagnetic simulations, analytical calulations and experiments, which includes Refs. [44–53].
[44] H. Stoll, M. Noske, M. Weigand, K. Richter, B. Krüger, R. M. Reeve, M. Hänze, C. F. Adolff, F.-U. Stein, G. Meier, M. Kläui, and G. Schütz, Imaging spin dynamics on the nanoscale using x-ray microscopy, Front. Phys. **3**, 26 (2015).
[45] S. Bonetti, R. Kukreja, Z. Chen, D. Spoddig, K. Ollefs, C. Schöppner, R. Meckenstock, A. Ney, J. Pinto, R. Houanche, J. Frisch, J. Stöhr, H. A. Dürr, and H. Ohldag, Microwave soft x-ray microscopy for nanoscale magnetization dynamics in the 5-10 GHz frequency range, Rev. Sci. Instrum. **86**, 093703 (2015).
[46] G. Schütz, W. Wagner, W. Wilhelm, P. Kienle, R. Zeller, R. Frahm, and G. Materlik, Absorption of Circularly Polarized X Rays in Iron, Phys. Rev. Lett. **58**, 737 (1987).
[47] L. Landau and E. Lifshits, On the theory of the dispersion of magnetic permeability in ferromgnetic bodies, Phys. Zeitschrift. der Sow. **8**, 153 (1935).
[48] T. L. Gilbert, A Lagrangian formulation of the gyromagnetic equation of the magnetization field, Phys. Rev. **100**, 1243 (1955).
[49] T. L. Gilbert, A phenomenological theory of damping in ferromagnetic materials, IEEE Trans. Magn. **40**, 3443 (2004).
[50] A. Vansteenkiste, J. Leliaert, M. Dvornik, M. Helsen, F. Garcia-Sanchez, and B. Van Waeyenberge, The design and verification of MuMax3, AIP Adv. **4**, 107133 (2014).
[51] J. Wei, Z. Zhu, C. Song, H. Feng, P. Jing, X. Wang, Q. Liu, and J. Wang, Annealing influence on the exchange stiffness constant of Permalloy films with stripe domains, J. Phys. D **49**, 265002 (2016).
[52] M. Dvornik, Y. Au, and V. V. Kruglyak, Micromagnetic simulations in magnonics, Top. Appl. Phys. **125**, 101 (2013).
[53] A. A. Thiele, Steady-State Motion of Magnetic Domains, Phys. Rev. Lett. **30**, 230 (1973).
[54] T. Shinjo, T. Okuno, R. Hassdorf, K. Shigeto, and T. Ono, Magnetic vortex core observation in circular dots of permalloy, Science **289**, 930 (2000).
[55] S.-B. Choe, Y. Acremann, A. Scholl, A. Bauer, A. Doran, J. Stöhr, and H. A. Padmore, Vortex core-driven magnetization dynamics, Science **304**, 420 (2004).
[56] M. Kammerer, M. Weigand, M. Curcic, M. Noske, M. Sproll, A. Vansteenkiste, B. Van Waeyenberge, H. Stoll, G. Woltersdorf, C. H. Back, and G. Schütz, Magnetic vortex core reversal by excitation of spin-waves, Nat. Commun. **2**, 279 (2011).
[57] R. V. Verba, A. Hierro-Rodriguez, D. Navas, J. Ding, X. M. Liu, A. O. Adeyeye, K. Y. Guslienko, and G. N. Kakazei, Spin-wave excitation modes in thick vortex-state circular ferromagnetic nanodots, Phys. Rev. B **93**, 214437 (2016).
[58] J. Ding, G. N. Kakazei, L. Liu, K. Y. Guslienko, and A. O. Adeyeye, Higher-order vortex gyrotropic modes in circular ferromagnetic nanodots, Sci. Rep. **4**, 4796 (2014).
[59] A. Vansteenkiste, K. W. Chou, M. Weigand, M. Curcic, V. Sackmann, H. Stoll, T. Tyliszczak, G. Woltersdorf, C. H. Back, G. Schütz, and B. Van Waeyenberge, X-ray imaging of the dynamic magnetic vortex core deformation, Nat. Phys. **5**, 332 (2009).
[60] S. J. Hermsdoerfer, H. Schultheiss, C. Rausch, S. Schäfer, B. Leven, S.-K. Kim, and B. Hillebrands, A spin-wave frequency doubler by domain wall oscillation, Appl. Phys. Lett. **94**, 223510 (2009).
[61] K.-S. Lee, S. Choi, and S.-K. Kim, Radiation of spin-waves from magnetic vortex cores by their dynamic motion and annihilation processes, Appl. Phys. Lett. **87**, 192502 (2005).
[62] S. Choi, K.-S. Lee, K. Yu. Guslienko, and S.-K. Kim, Strong Radiation of Spin-waves by Core Reversal of a Magnetic Vortex and Their Wave Behaviors in Magnetic Nanowire Waveguides, Phys. Rev. Lett. **98**, 087205 (2007).

[63] B. Mozooni and J. McCord, Direct observation of closure domain wall mediated spin-waves, Appl. Phys. Lett. **107**, 042402 (2015).

[64] V. Sluka, M. Weigand, A. Kakay, A. Erbe, V. Tyberkevych, A. Slavin, A. Deac, J. Lindner, J. Fassbender, J. Raabe, and S. Wintz, Stacked topological spin textures as emitters for multidimensional spin wave modes, *Proceedings of IEEE International Magnetics Conference (INTERMAG), Beijing, 2015* (IEEE, New York, 2015).

[65] B. Van de Wiele, S. J. Hämäläinen, P. Baláž, F. Montoncello, and S. van Dijken, Tunable short-wavelength spin wave excitation from pinned magnetic domain walls, Sci. Rep. **6**, 21330 (2016).

[66] N. J. Whitehead, S. A. R. Horsley, T. G. Philbin, A. N. Kuchko, and V. V. Kruglyak, Theory of linear spin wave emission from a Bloch domain wall, Phys. Rev. B **96**, 064415 (2017).